AGU PUBLICATIONS

Geophysical Research Letters

RESEARCH LETTER
10.1002/2017GL074471

**Key Points:**
- Magnetic fabrics display the same transport directions as inferred from structural analyses of slumped Mass Transport deposits (MTDs)
- A robust procedure to infer MTDs transport directions is outlined based on analyses of magnetic fabrics within slumped MTDs
- Magnetic fabrics and anisotropy variations in drill cores may reflect deformation within individual MTDs rather than separate MTDs

**Correspondence to:**
R. Weinberger,
rami.weinberger@gsi.gov.il

**Citation:**
Weinberger, R., T. Levi, G. I. Alsop, and S. Marco (2017), Kinematics of Mass Transport Deposits revealed by magnetic fabrics, *Geophys. Res. Lett.*, *44*, doi:10.1002/2017GL074471.

Received 11 JUN 2017
Accepted 20 JUL 2017
Accepted article online 26 JUL 2017



# Kinematics of Mass Transport Deposits revealed by magnetic fabrics

**R. Weinberger[1,2], T. Levi[1], G. I. Alsop[3], and S. Marco[4]**

[1]Geological survey of Israel, Jerusalem, Israel, [2]Department of Geological and Environmental Sciences, Ben-Gurion University of the Negev, Beer Sheva, Israel, [3]Department of Geology and Petroleum Geology, School of Geosciences, University of Aberdeen, Aberdeen, UK, [4]Department of Geophysics, School of Geosciences, Tel Aviv University, Tel Aviv, Israel

**Abstract** The internal deformation and movement directions of Mass Transport Deposits (MTDs) are key factors in understanding the kinematics and dynamics of their emplacement. Although these are relatively easy to recover from well-bedded sediments, they are more difficult to deduce from massive beds without visible strain markers. In order to test the applicability of using anisotropy of magnetic susceptibility (AMS) to determine MTD movement, we compare AMS fabrics, with structural measurements of visible kinematic indicators. Our case study involves the structural analysis of slumped lake sediments extensively exposed in MTDs within the Dead Sea Basin. Structural analyses of MTDs outcropping for >100 km reveal radial transport directions toward the basin depocenter. We show that the AMS fabrics display the same transport directions as inferred from structural analyses. Based on this similarity, we outline a robust procedure to obtain the transport direction of slumped MTDs from AMS fabrics. Variations in the magnetic fabrics and anisotropies in fold-thrust systems within the slumps match the various structural domains. We therefore suggest that magnetic fabrics and anisotropy variations in drill cores may reflect internal deformation within the slumps rather than different slumps. Obtaining magnetic fabrics from MTDs provides a viable way to infer the transport directions and internal deformation of MTDs and reconstruct the basin depocenter in ancient settings. The present results also have implications beyond the kinematics of MTDs, as their geometry resembles fold-thrust systems in other geological settings, scales, and tectonic environments.

## 1. Introduction

Mass Transport Deposits (MTDs) are associated with large-scale hazardous processes such as tsunamis and earthquakes resulting in losses of life, property, and infrastructure. Hence, recent studies aim to infer the transport directions and internal deformation of MTDs, as these are key factors in understanding the kinematics and dynamics of their formation. Structural analyses of MTDs can reveal the transport directions and internal strain variations but are largely based on visible strain markers such as displaced bedding planes. In massive sediments, where strain markers are not readily identified, an alternative approach is needed. In this study, we analyze the anisotropy of magnetic susceptibility (AMS) of finely laminated MTDs and show how the structural analysis corresponds to AMS measurements.

AMS-based analysis is used in sedimentary rocks for characterizing petrofabrics and quantifying weak internal deformation [e.g., *Hrouda,* 1982; *Averbuch et al*., 1992; *Schwehr and Tauxe*, 2003; *Borradaile and Jackson*, 2004; *Parés*, 2015]. The maximum $K_1$, intermediate $K_2$, and minimum $K_3$ magnetic susceptibility axes correspond to $k_1$, $k_2$, and $k_3$ eigenvalues of the AMS. The $K_1$ and $K_3$ axes are generally parallel to the long and short axes of particle shapes, respectively. When deposited in still water, elongate particles tend to lie parallel to the horizontal bedding plane, forming a "deposition fabric." In this fabric, the $K_1$ and $K_2$ axes lie within the bedding plane and are indistinguishable, while the $K_3$ axes are well clustered and vertical. Where water was flowing, the $K_1$ axes typically cluster about the flow direction, but under certain conditions $K_1$ axes may align perpendicular to flow direction [e.g., *Tarling and Hrouda*, 1993]. During later deformation within MTDs, the original fabric might evolve into a deformation fabric, in which the $K_1$ and $K_2$ axes are well clustered and clearly distinguishable (i.e., 95% confidence ellipses do not overlap).

In marine environments, deep-sea drilling provides almost the sole opportunity to observe the details of recent MTDs continuously [e.g., *Bull et al*., 2009; *Gamboa et al*., 2010, and reference therein]. These studies

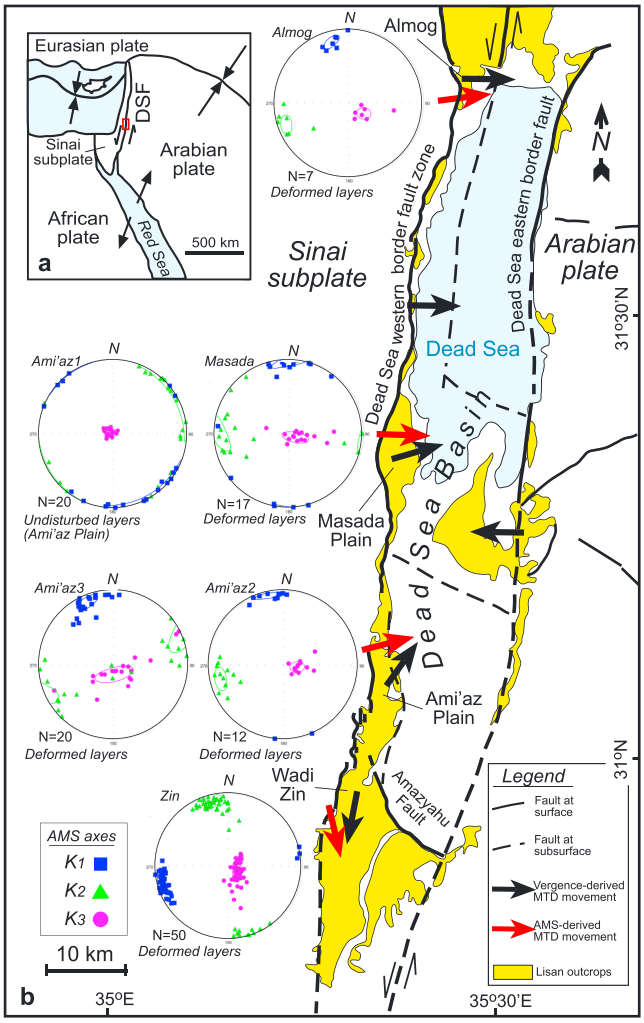


**Figure 1.** (a) General tectonic map showing the location of the study area (small red box) along the Dead Sea Fault (DSF) system. (b) Map of the Dead Sea Basin showing outcrops of the Lisan Formation and the position of strands of the DSF system. Black arrows represent the direction of slumping in MTDs within the Lisan Formation based on the structural measurements along the western side [*Alsop and Marco*, 2012] and eastern margin [*El-Isa and Mustafa*, 1986] of the Dead Sea. Red arrows represent the direction of the slumping in MTDs based on the present AMS analysis. Stereoplots are lower hemisphere, equal-area projection of AMS principal axes, and the 95% confidence ellipses. Blue squares, green triangles, and pink circles represent the $K_1$, $K_2$, and $K_3$ axes, respectively.

suffer from having very narrow windows of observation (a few centimeters across) that may hamper the kinematic interpretation. A few previous studies [*Schwehr et al.*, 2007; *Meissl et al.*, 2011; *Kanamatsu et al.*, 2014] have taken advantage of the continuous cores through MTDs, to portray their kinematics with AMS. Such studies have to use available paleomagnetic data in order to reconstruct the transport directions of MTDs. In contrast with outcrop studies, the limited core volume generally precludes collection of enough sample material to obtain a statistically significant interpretation of AMS variations through the sequence. Hence, ground truthing of the slumping process based on AMS studies in a wider, well-exposed outcrop-based study is timely and necessary.

In this study, we compare magnetic fabrics with structural observations recorded from slumped MTDs. We take advantage of the exceptionally well-exposed recent (<40 kyr) MTDs in lake deposits within the Dead Sea Basin (DSB). Along-strike exposures extending for over 100 km display radial transport directions toward the depocenter [*Alsop and Marco*, 2012] (Figure 1) and provide an ideal case study to test whether the magnetic fabrics generated during slumping indicate the absolute transport direction of MTDs. We quantify the internal deformation within the slumps and examine the possibility that different particles (e.g., carbonates, clays, and iron-rich particles) within MTDs accommodate the strain differently. Our results have a direct bearing on inferring transport directions and internal deformation within MTDs, the potential location of basin depocenters in ancient settings, and providing an independent test of the structural interpretation in these systems.

## 2. Geologic Setting

The DSB is a pull-apart structure (Figure 1a) developed between two left-stepping strands of the Dead Sea Fault (DSF) system [*Garfunkel*, 1981; *Quennell*, 1956]. It has been seismically active since the early Miocene [*Nuriel et al.*, 2017] until the present. Past earthquakes triggered coseismic deformation [*Marco and Agnon*, 1995; *Weinberger et al.*, 2016] and subaqueous MTDs within the Lisan Formation [*El-Isa and Mustafa*, 1986; *Alsop et al.*, 2017].

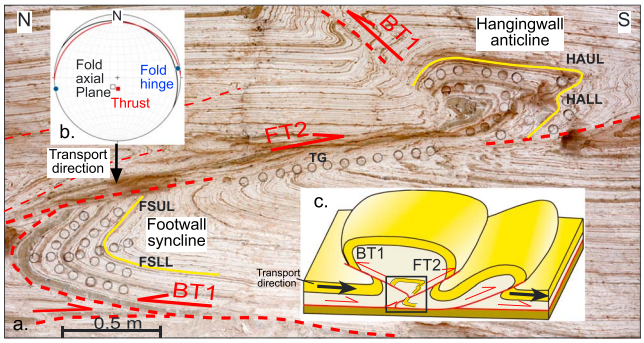


**Figure 2.** (a) Photo of fold-thrust systems in Wadi Zin (Figure 1b), showing the sampling scheme for the magnetic study. Specimens seen as circles in this cross section were taken from the footwall syncline (FSUL—upper limb; FSLL—lower limb), fault gouge zone (TG), and hanging wall anticline (HAUL—upper limb; HALL—lower limb) of the fold-thrust system. Dashed red lines mark the location of fore thrust (FT2) and back thrust (BT1). (b) Lower hemisphere, equal-area stereoplot showing structural data from the fold-thrust system, and the inferred transport direction. (c) Three-dimensional cartoon illustrating the studied slump and the sequential relationships between the BT1 and the FT2 in this site. Black rectangle schematically represents the studied area in Figure 2a.

The exposed lacustrine sediments of the Lisan Formation comprise an ~40 m sequence of alternating white authigenic aragonite and fine dark detrital laminae dated to 70–15 ka [*Haase-Schramm et al*., 2004]. The aragonite precipitated chemically from the upper surface of Lake Lisan (the precursor of the Dead Sea), whereas the fine detritus, which contains mainly clay minerals, was carried by annual floods. The lacustrine sediments are currently widely exposed within the DSB (Figure 1b) due to significant shrinkage of Lake Lisan at 14–11 kyr. These exposures reveal well-developed soft-sediment slumps, comprising fold-thrust systems. Individual slump sheets are typically $<2$ m thick and are capped by undeformed horizontal beds, indicating that the fold-thrust systems affect soft sediments formed at the near surface, rather than related to any later tectonic deformation of a lithified sequence.

The transport directions of MTDs exposed around the DSB were inferred using field measurements of fold hinges and axial planes. These measurements were used to deduce the downslope/transport direction under several basic assumptions; e.g., fold hinges form at right angles to the downslope direction and produce statistical grouping normal to the transport direction [*Alsop and Marco*, 2012]. The systematic regional patterns are consistent with MTD emplacement being controlled by gravity-driven movement toward the depocenter of a basin. Slumps in Wadi Zin, south of the transversal Amazyahu Fault (Figure 1b), show southward directed transport away from the depocenter (Figure 2), suggesting that sediments were tilted gently southward on large fault blocks during seismically triggered slumping.

## 3. Magnetic Fabrics of the Lisan Slumps

The Lisan Formation aragonite and detrital laminae are diamagnetic and paramagnetic, respectively, while the bulk AMS susceptibility is typically positive. Titanomagnetite, magnetite, and greigite are the ferromagnetic carrier in the detrital laminae [e.g., *Ron et al*., 2006; *Levi et al*., 2006a, 2014]. We sampled 126 specimens from six outcrops (Figure 1b), one of which consists of undisturbed layers for reference (Ami'az1; Figure 1b), while the others comprise fold-thrust systems in MTDs that previously were studied by structural analyses [*Alsop and Marco*, 2012]. An intensive sampling was carried out in Wadi Zin (Figure 1b), which consists of a superb example of fault-propagation folds (FPFs) that formed during slumping. In this locality we sampled separate layers in the hanging wall anticline and footwall syncline, as well as in gouge zones along thrusts (Figure 2). The AMS was measured with a KLY-4S Kappabridge and the anisotropy of anhysteretic remanent magnetization (AARM) with alternating field demagnetizer/magnetizer, LDA-3/AMU-1, and a JR-6 spinner magnetometer (*AGICO Inc*., Czech Republic) at the Geological Survey of Israel. The AARM provides information on the petrofabric of remanence-bearing particles, where $K_R$ is the magnetic susceptibility of the remanence [*Martín-Hernández and Ferré*, 2007]. Protocols of measurements and parametric analyses are given in *Levi et al*. [2014].

## 4. Results

We found that all samples have positive bulk AMS susceptibility, with site mean $k_m$ ranging between 20 and $100 \times 10^{-6}$ SI (Table 1). The AMS fabric of the undisturbed layers in the Ami'az Plain is characterized by a deposition fabric, in which the 95% confidence ellipses of the subhorizontal $K_1$ and $K_2$ axes overlap, and

**Table 1.** AMS and AARM Data[a]

| Site | N | $K_m$ (STD) | $L$ (STD) | $F$ (STD) | $P_j$ (STD) | $T$ (STD) | $D, I$ of $K_1$ (Half Confidence Angles) | $D, I$ of $K_2$ (Half Confidence Angles) | $D, I$ of $K_3$ (Half Confidence Angles) |
|---|---|---|---|---|---|---|---|---|---|
| Almog | 7 | 63.1 | 1.010 | 1.014 | 1.020 | 0.108 | 344, 16 | 250, 12 | 124, 69 |
| | | (10.6) | (0.003) | (0.009) | (0.008) | (0.361) | (14.6/5.5) | (18.3/8.8) | (14.9/5.6) |
| Masada | 17 | 23.6 | 1.009 | 1.024 | 1.035 | 0.454 | 360, 05 | 269, 08 | 119, 80 |
| | | (10.1) | (0.007) | (0.009) | (0.008) | (0.407) | (9.4/4.6) | (9.4/4.6) | (9.4/4.6) |
| Ami'az1 (undisturbed) | 20 | 48.2 | 1.002 | 1.024 | 1.029 | 0.872 | 149, 02 | 059, 02 | 280, 87 |
| | | (11.5) | (0.001) | (0.002) | (0.003) | (0.058) | (37.8/2.9) | (37.8/3.8) | (4.0/3.6) |
| Ami'az2 | 12 | 25.8 | 1.018 | 1.019 | 1.038 | 0.036 | 349, 06 | 257, 15 | 098, 74 |
| | | (8.8) | (0.011) | (0.008) | (0.010) | (0.398) | (11.3/3.7) | (10.5/8.0) | (8.1/5.6) |
| Ami'az2 (AARM) | 10 | 23.2 | 1.059 | 1.086 | 1.153 | 0.147 | 359, 03 | 268, 15 | 100, 74 |
| | | (8.5) | (0.020) | (0.035) | (0.029) | (0.320) | (12.8/3.5) | (15.2/11.6) | (14.61/4.9) |
| Ami'az3 | 20 | 99.7 | 1.016 | 1.014 | 1.031 | −0.089 | 337, 11 | 068, 03 | 174, 79 |
| | | (82.1) | (0.005) | (0.008) | (0.008) | (0.352) | (10.5/6.6) | (21.4/8.8) | (21.3/7.5) |
| Zin | 50 | 21.3 | 1.018 | 1.024 | 1.043 | 0.149 | 256, 09 | 347, 08 | 120, 78 |
| | | (8.8) | (0.007) | (0.007) | (0.009) | (0.280) | (9.4/4.6) | (11.0/8.4) | (10.4/4.1) |
| Zin (AARM-folds) | 29 | 15.8 | 1.048 | 1.075 | 1.129 | 0.204 | 275, 02 | 005, 07 | 171, 83 |
| | | (4.8) | (0.012) | (0.017) | (0.016) | (0.200) | (9.4/5.3) | (12.1/9.3) | (12.4/4.5) |
| Zin (AARM-thrusts) | 16 | 20.8 | 1.018 | 1.101 | 1.120 | 0.667 | 271, 05 | 181, 01 | 080, 85 |
| | | (5.5) | (0.012) | (0.026) | (0.017) | (0.268) | (25.4/4.5) | (25.5/6.4) | (7.2/4.4) |

[a]$N$, number of specimens; $k_m$, mean susceptibility (in $10^{-6}$ SI units); $L$, lineation; $Pj$, corrected anisotropy degree; $T$, shape ellipsoid; $D, I$ of $K_i$, declination and inclination of the susceptibility axis ($i$ = 1, 2, and 3). STD—standard deviation and half confidence angles are in parentheses (Jelinek's statistics).

the $K_3$ axes are tightly clustered and vertical (Ami'az1 site; Figure 1b). The AMS fabrics of the deformed layers at all outcrops are characterized by a "deformation fabric" (Figure 1b). The $K_1$ and $K_2$ axes are subhorizontal and well clustered relative to these axes in the reference fabric (Almog, Ami'az2, Ami'az3, and Wadi Zin sites in Figure 1b). Many of the $K_3$ axes are off vertical, showing a trail of axes directed toward the transport direction (e.g., Masada site; Figure 1b), forming a weak magnetic girdle of $K_2$ and $K_3$ axes (Ami'az3 site; Figure 1b). In Wadi Zin, deviation of the $K_3$ axes from the vertical is more distinct in specimens taken from the hanging wall anticline and hinges in the footwall syncline. The AARM fabrics from Wadi Zin are divided into two populations: (1) specimens from the folds (Figure 3a) and (2) specimens from the gouge zones along thrusts (Figure 3b). Similar to the AMS fabric from Wadi Zin, the AARM fabric of the folds is characterized by a deformation fabric, in which $K_{R1}$ and $K_{R2}$ axes are subhorizontal and well clustered, with many of the $K_{R3}$ axes off vertical. A comparison between the AMS (Figure 1b) and AARM (Figure 3a) principal axes from the slump in Wadi Zin indicates that the AARM axes are directed ~15° clockwise relative to their respective AMS axes. The AARM principal axes of the gouge zones are less clustered than these from the folds, with many of the $K_{R1}$ and $K_{R2}$ axes being indistinguishable, although the 95% confidence ellipses do not overlap (Figure 3b). The AARM fabric from Ami'az2 site (Figure 3c) is quite similar to its respective AMS fabric (Figure 1b), but the trail of $K_{R3}$ axes toward the girdle is more distinct and associated with a very elongated, W-E oriented 95% confidence ellipse. AMS data of lineation ($L = k_1/k_2$) versus foliation ($F = k_2/k_3$) from the Wadi Zin site shows that all specimens from the thrust gouge have an oblate shape, whereas a few specimens from the hinges and the hanging wall anticline have a well-defined prolate shape (Figure 4 and Table 1).

## 5. Discussion

The AMS fabric of the undisturbed Lisan bedding is a classic deposition fabric (Ami'az1, Figure 1b). This pre-slumped, original fabric is significantly different from the deformation fabrics of the Lisan MTDs. The latter fabrics were obtained from five different sites along the DSB and are associated with varied vergence of fold-thrust systems. These MTDs were not deformed by postslumping tectonics, indicating that their fabric has not been obliterated after slumping. Regardless of the site location, all AMS fabrics of the MTDs have the following common affinities to the transport direction as inferred from the structural analysis: (1) $K_1$ axes are oriented normal to the axis of the transport direction (i.e., parallel to the fold hinges and strikes of thrusts); (2) $K_2$ axes are parallel to the axis of the transport direction; and (3) $K_3$ axes deviate from the vertical, showing

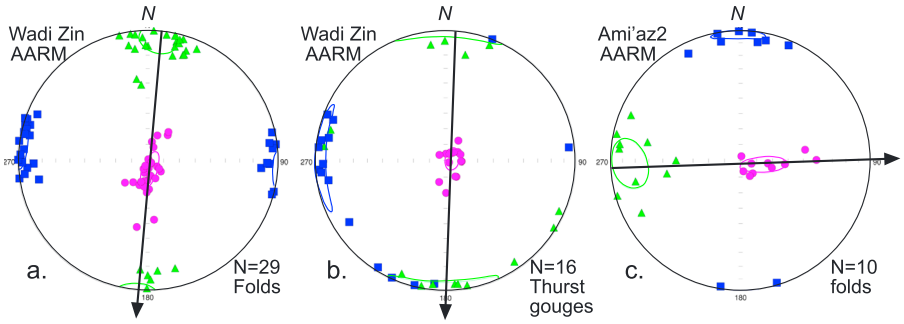


**Figure 3.** (a–c) Lower hemisphere, equal-area projection stereoplots of AARM principal axes, and the 95% confidence ellipses. The $K_{R1}$, $K_{R2}$, and $K_{R3}$ axes are denoted by blue squares, green triangle, and pink circles, respectively. Stereoplot in Figure 3a is from the footwall syncline and hanging wall anticline in Wadi Zin. Stereoplot in Figure 3b is from gouge zone along thrusts in Wadi Zin. Stereoplot in Figure 3c is from the slump in Almog. The inferred transport direction is indicated by black arrows (see text).

a trail of axes, which are commonly directed toward the absolute transport direction [e.g., *Parés*, 2015]. Based on these characteristics, we suggest that the transport direction of slumped MTDs could be confidently estimated from AMS data by a two-step procedure (Figure 3c). First, a great circle containing the means of the $K_2$ and $K_3$ axes is calculated and the strike of this plane approximates to the axis of the transport direction. Next, the absolute transport direction is inferred based on the directional deviation of $K_3$ from verticality. Accordingly, most of the area of the 95% confidence ellipses (Figure 1b) and the bootstrapped replicates lie in the quadrangle of the absolute transport direction, highlighting this direction over the opposing azimuth. Likewise, the transport direction of slumped MTDs can be obtained from AARM data (Figure 3) with the most instructive example from the Ami'az2 site (Figure 3c). In Ami'az3 site (Figure 1b), the $K_2$ and $K_3$ axes form a weak magnetic girdle that might evolve due to rollover of some particles, resulting in the $K_3$ axes pointing toward the opposing azimuth of the transport direction [e.g., *Levi et al.*, 2006a, 2006b]. Such a fabric, although exceptional in this study, highlights the possibility that more evolved fabrics may hinder the determination of the absolute transport direction without general knowledge on the location of the depocenter.

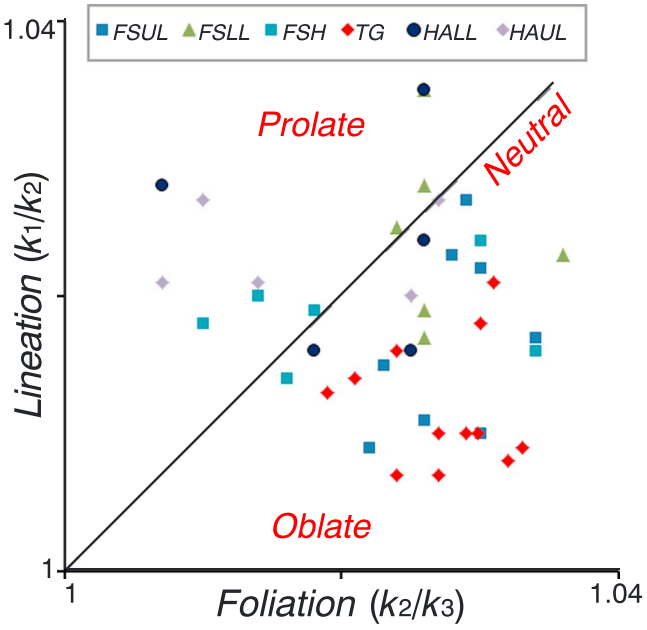


**Figure 4.** Flinn's plot (Lineation = $k_1/k_2$ versus foliation = $k_2/k_3$) of AMS data from different structural domains of the fold-thrust structure in Wadi Zin. See Figure 2 for location and legend.

Our results characteristically show that the mean of $K_2$ axes are nearly antiparallel to the absolute transport direction. However, ambiguity still remains as to whether this direction could be inferred from the means of the $K_1$ or $K_2$ axes alone. *Schwehr et al.* [2007] found that the expected direction of contraction based on morphology closely matches the direction of contraction from AMS axes [*Schwehr et al.*, 2007, Figure 18]. More specifically, this direction contains the mean of $K_2$ axes and a trail of $K_3$ axes, similar to the present case study. *Kanamatsu et al.* [2014] reconstructed the shear direction of six submarine MTDs from AMS data. In one of these MTDs, they inferred a direction based on the $K_1$ and $K_3$ axes, while for the other five, a direction that contains the $K_2$ and $K_3$ axes was

inferred. *Meissl et al*. [2011] deduced that the $K_3$ axes would deviate from the vertical toward the direction of transport, and the mean of $K_1$ axes provides the first-order interpretation of the MTD movement direction.

Bedding-parallel shearing during slumping would tend to physically rotate particles along horizontal axes in such a way that in a lower hemisphere projection, rotation would result in the particle short axes pointing toward the transport direction [*Rees*, 1965]. Because the particle short and long axes are likely to coincide with the direction of the minimum and maximum susceptibility axes, respectively, the magnetic fabrics of slumped sediments have trails of $K_3$ and $K_{R3}$ axes pointing toward the transport direction but well-clustered $K_1$ and $K_{R1}$ axes parallel to the fold hinges. Three types of particles contribute to the bulk susceptibility of the Lisan Formation: diamagnetic needles of aragonite, paramagnetic plates of clays, and accessory ferromagnetic titanomagnetite, magnetite, and greigite [e.g., *Ron et al*., 2006]. In general, the AMS and AARM fabrics are quite similar, but in detail there are some differences, e.g., the trail of $K_3$ axes are more distinct in the AARM fabrics (Figure 3c versus Figure 1b), with a ~15° difference between the directions of $K_i$ and $K_{Ri}$ in Wadi Zin. This indicates that the ferromagnetic particles (in a broad sense) accommodate the strain during slumping somewhat differently than the aragonite needles and clay plates.

The alignment of all particles in the Lisan MTDs is due to a simple coaxial kinematic history, so the AMS ellipsoid for all particles and the AARM ellipsoid for remanence-bearing particles apparently should be the same. This is not strictly the case in Wadi Zin and Amia'z2 sites, although it is evident that the deformation was synchronous and coaxial. We suggest that during slumping the more spherical particles of (titano)magnetite were easily aligned parallel to the fold hinges and normal to the transport direction. They might collectively form an elongation shape in the direction of $K_{R1}$ and parallel to the fold hinges and distinct trail of $K_{R3}$ axes in the direction of transportation. However, the nonspherical aragonite needles and clay plates statistically were not always fully rotated parallel to the fold hinges. This may reflect in variations of ~15° between the AMS-derived and vergence-derived MTD transport directions. Comparison between the $K_{Ri}$ axes with structural axes, such as fold hinges and thrust strikes in Wadi Zin, indicates that the AARM principal axes might be more faithful recorders of the transport direction in the slumped Lisan case study. Hence, phase separation and in particular obtaining AARM fabrics of MTDs are required in order to better interpret the kinematic of MTDs during slumping. Previous studies have shown ambiguity as to whether the $K_1$ or $K_2$ axes lie along the transport direction. This ambiguity may be the result of differences in the physical shape and properties of particles in MTDs from various environments, the more magnetic of which control the direction of the bulk AMS axes.

The MTDs in the Lisan Formation are composed of fold-thrust systems, which formed typical fault propagation folds (FPFs) [*Alsop et al*., 2017]. In this system, the AMS fabrics of the thrust gouge are always oblate, whereas those in the hanging wall anticline and the hinges of the footwall syncline are more prolate (Figure 4). The prolate fabric could be created by originally oblate thrust-related fabrics being rotated during folding [*Fossen*, 2016, p. 69]. This variation of the magnetic fabrics throughout the sequence is related to the heterogeneous strain distribution within FPF systems as known from different scales and geologic settings [e.g., *Averbuch et al*., 1992]. The consequence is that in vertical cores recovered from submarine MTDs, anisotropy variations throughout the core may arise because of the possibility of drilling down from the hanging wall anticline through thrust gouge and into the underlying footwall syncline. These anisotropy variations reflect the distribution of internal deformation within the same slumped system and not necessarily changes between adjacent slumped systems and different transport directions.

## 6. Conclusions

Based on the similar results of magnetic fabrics and structural analyses of slumped MTDs in the Lisan Formation MTDs around the DSB, we conclude that the transport direction of slumped MTDs can be estimated reliably by a two-step procedure. First, a great circle containing the means of the $K_2$ ($K_{R2}$) and $K_3$ ($K_{R3}$) axes is calculated and the strike of this plane approximates to the axis of the transport direction. Second, the absolute transport direction is determined based on the deviation of the $K_3$ ($K_{R3}$) from verticality. Different types of particles within the slumped MTDs are oriented somewhat differently, depending on their physical shape and properties. Ferromagnetic particles may accommodate the strain more fully than other particles and serve as a faithful kinematic indicator for the transport direction. Hence, obtaining AARM fabrics from MTDs adds an important component in assessing their kinematics. We show that anisotropy variations

may reflect the distribution of internal deformation within the same slump rather than changes between adjacent slumps. Many continental slope regions are associated with slope failure and MTDs. Obtaining magnetic fabrics from these MTDs provides a practical way to infer their transport directions and internal deformation and potentially the location of paleobasin depocenters.

**Acknowledgments**
This study was supported by the Israel Science Foundation (ISF grants 868/17 and 1436/14). We thank the Editor A.V. Newman and the reviewers M. Jackson and B. Almqvist, whose comments and suggestions improved the quality of our manuscript. The laboratory assistance of Ran Issachar and Daniel Zvi is highly acknowledged. All data used in this analysis are presented in Figures 1–4 and Table 1. Correspondence and requests for materials should be addressed to R.W. (rami.weinberger@gsi.gov.il).

## References

Alsop, G. I., and S. Marco (2012), A large-scale radial pattern of seismogenic slumping towards the Dead Sea Basin, *J. Geol. Soc.*, *169*(1), 99–110.
Alsop, G. I., S. Marco, T. Levi, and R. Weinberger (2017), Fold and thrust systems in Mass Transport Deposits, *J. Struct. Geol.*, *94*, 98–115.
Averbuch, O., D. F. de Lamotte, and C. Kissel (1992), Magnetic fabric as a structural indicator of the deformation path within a fold-thrust structure: A test case from the Corbières (NE Pyrenees, France), *J. Struct. Geol.*, *14*(4), 461–474.
Borradaile, G. J., and M. Jackson (2004), Anisotropy of magnetic susceptibility (AMS): Magnetic petrofabrics of deformed rocks, *Geol. Soc. London Spec. Publ.*, *238*(1), 299–360.
Bull, S., J. Cartwright, and M. Huuse (2009), A review of kinematic indicators from mass-transport complexes using 3D seismic data, *Mar. Petrol. Geol.*, *26*(7), 1132–1151.
El-Isa, Z. H., and H. Mustafa (1986), Earthquake deformations in the Lisan deposits and seismotectonic implications, *Geophys. J. Int.*, *86*(2), 413–424.
Fossen, H. (2016), *Structural Geology*, 463 pp., Cambridge Univ. Press, Cambridge.
Gamboa, D., T. Alves, J. Cartwright, and P. Terrinha (2010), MTD distribution on a "passive" continental margin: The Espírito Santo Basin (SE Brazil) during the Palaeogene, *Mar. Petrol. Geol.*, *27*(7), 1311–1324.
Garfunkel, Z. (1981), Internal structure of the Dead Sea leaky transform (rift) in relation to plate kinematics, *Tectonophysics*, *80*(1–4), 81–108.
Haase-Schramm, A., S. L. Goldstein, and M. Stein (2004), U-Th dating of Lake Lisan (late Pleistocene Dead Sea) aragonite and implications for glacial East Mediterranean climate change, *Geochim. Cosmochim. Acta*, *68*(5), 985–1005.
Hrouda, F. (1982), Magnetic anisotropy of rocks and its application in geology and geophysics, *Geophys. Surv.*, *5*(1), 37–82.
Kanamatsu, T., K. Kawamura, M. Strasser, B. Novak, and Y. Kitamura (2014), Flow dynamics of Nankai Trough submarine landslide inferred from internal deformation using magnetic fabric, *Geochem. Geophys. Geosyst.*, *15*, 4079–4092, doi:10.1002/2014GC005409.
Levi, T., R. Weinberger, T. Aïfa, Y. Eyal, and S. Marco (2006a), Injection mechanism of clay-rich sediments into dikes during earthquakes, *Geochem. Geophys. Geosyst.*, *7*, Q12009, doi:10.1029/2006GC001410.
Levi, T., R. Weinberger, T. Aïfa, Y. Eyal, and S. Marco (2006b), Earthquake-induced clastic dikes detected by anisotropy of magnetic susceptibility, *Geology*, *34*(2), 69–72.
Levi, T., R. Weinberger, and S. Marco (2014), Magnetic fabrics induced by dynamic faulting reveal damage zone sizes in soft rocks, Dead Sea basin, *Geophys. J. Int.*, *199*(2), 1214–1229.
Marco, S., and A. Agnon (1995), Prehistoric earthquake deformations near Masada, Dead Sea graben, *Geology*, *23*(8), 695–698.
Martín-Hernández, F., and E. C. Ferré (2007), Separation of paramagnetic and ferromagnetic anisotropies: A review, *J. Geophys. Res.*, *112*, B03105, doi:10.1029/2006JB004340.
Meissl, S., J. H. Behrmann, and C. Franke (2011), Magnetic fabrics in Quaternary sediments, Ursa Basin, northern Gulf of Mexico record transport processes, compaction and submarine slumping, *Mar. Geol.*, *286*(1), 51–64.
Nuriel, P., R. Weinberger, A. R. C. Kylander-Clark, B. R. Hacker, and J. P. Craddock (2017), The onset of the Dead Sea transform based on calcite age-strain analyses, *Geology*, *45*(7), 587–590, doi:10.1130/G38903.1.
Parés, J. M. (2015), Sixty years of anisotropy of magnetic susceptibility in deformed sedimentary rocks, *Front. Earth Sci.*, *3*, 4.
Quennell, A. M. (1956), Tectonics of the Dead Sea Rift, in *Proceedings Congreso Geologico Internacional, 20th Sesión*, pp. 385–405, Asociación de Servicios Geologicos Africanos, Mexico City.
Ron, H., N. R. Nowaczyk, U. Frank, S. Marco, and M. O. McWilliams (2006), Magnetic properties of Lake Lisan and Holocene Dead Sea sediments and the fidelity of chemical and detrital remanent magnetization, *Geol. Soc. Am. Spec. Pap.*, *401*, 171–182.
Schwehr, K., and L. Tauxe (2003), Characterization of soft-sediment deformation: Detection of cryptoslumps using magnetic methods, *Geology*, *31*(3), 203–206.
Schwehr, K., N. Driscoll, and L. Tauxe (2007), Origin of continental margin morphology: Submarine-slide or downslope current-controlled bedforms, a rock magnetic approach, *Mar. Geol.*, *240*(1–4), 19–41.
Tarling, D., and F. Hrouda (1993), *The Magnetic Anisotropy of Rocks*, 217 pp., Chapman and Hall, London.
Weinberger, R., T. Levi, G. I. Alsop, and Y. Eyal (2016), Coseismic horizontal slip revealed by sheared clastic dikes in the Dead Sea Basin, *Geol. Soc. Am. Bull.*, *128*(7–8), 1193–1206.